

Resistive MHD stability studies for LHD configurations

Luis GARCIA¹⁾, Jacobo VARELA¹⁾ and Kiyomasa WATANABE²⁾

¹⁾Universidad Carlos III, 28911 Leganés, Madrid, Spain

²⁾National Institute for Fusion Science, Toki, Gifu 509-5292, Japan

October 15, 2007

A set of reduced equations is derived without making any assumption on the number of field periods. The equilibrium used in the equations is the exact three-dimensional equilibrium without any average in the toroidal angle. Using this set of equations, we study the ideal and resistive MHD properties of different LHD configurations. The linear results are compared with the ones obtained from the full MHD equations in the pressure-convection limit. The agreement is very good.

Keywords: Resistive MHD, LHD, Reduced equations

1 Introduction

Pressure-driven instabilities are a key feature in stellarator stability, since no net toroidal current flows in the plasma, avoiding the appearance of current-driven instabilities. Modes with high poloidal wavenumber m are usually studied using the ballooning formalism, which reduces the stability problem to finding the eigenvalue of a system of differential equations to be solved along the magnetic lines. The stellarator expansion can be applied to study the stability of modes with low toroidal wavenumber n whose variation along field lines is slow compared with the variation of the stellarator terms. A reduced set of equations expressed in terms of the equilibrium flux coordinates was derived for those modes [1]. They are formally the same as the reduced set of MHD equations for a tokamak.

The calculation of global modes using the full three-dimensional equilibrium has been based on formulations of the ideal MHD energy principle in magnetic coordinates [2, 3]. However, these formulations cannot include the effect of resistivity and are not suitable for nonlinear calculations. In order to be able of studying the nonlinear evolution, we developed a numerical code (FAR3D), which solves the full set of resistive MHD equations [4].

2 Reduced Equations

For high-aspect ratio configurations with moderate β -values (of the order of the inverse aspect ratio), we can apply the method employed in Ref. [1] for the derivation of the reduced set of equations without averaging in the toroidal angle. In this way, we get a reduced set of equations using the exact three-dimensional equilibrium. In this formulation, we include linear helical couplings between mode components, which were not included in the formulation developed in Ref. [1].

The main assumptions for the derivation of the set of reduced equations are high aspect ratio, medium β (of the order of the inverse aspect ratio ε), small variation of the fields, and small resistivity. With these assumptions, we can write the velocity and perturbation of the magnetic field as

$$\mathbf{v} = \sqrt{g}R_0\nabla\zeta \times \nabla\Phi, \quad \mathbf{B} = R_0\nabla\zeta \times \nabla\psi, \quad (1)$$

where ζ is the toroidal angle, Φ is a stream function proportional to the electrostatic potential, and ψ is the perturbation of the poloidal flux.

The equations, in dimensionless form, are

$$\frac{\partial\psi}{\partial t} = \nabla_{\parallel}\Phi + \frac{\eta}{S}B_{\zeta}^{eq}J_{\zeta} \quad (2)$$

$$\begin{aligned} \frac{\partial U}{\partial t} = & -\mathbf{v} \cdot \nabla U + \frac{\beta_0}{2\varepsilon^2} \left(\frac{1}{\rho} \frac{\partial \sqrt{g}}{\partial \theta} \frac{\partial p}{\partial \rho} - \frac{\partial \sqrt{g}}{\partial \rho} \frac{1}{\rho} \frac{\partial p}{\partial \theta} \right) \\ & + \nabla_{\parallel}J^{\zeta} - \frac{1}{\rho} \frac{\partial}{\partial \rho} (\rho J_{eq}^{\zeta}) \frac{1}{\rho} \frac{\partial \psi}{\partial \theta} + \frac{1}{\rho} \frac{\partial J_{eq}^{\zeta}}{\partial \theta} \frac{\partial \psi}{\partial \rho} \end{aligned} \quad (3)$$

$$\frac{\partial p}{\partial t} = -\mathbf{v} \cdot \nabla p + \frac{dp_{eq}}{d\rho} \frac{1}{\rho} \frac{\partial \Phi}{\partial \theta} \quad (4)$$

Here, $U = \sqrt{g} \left[\nabla \times (\rho_m \sqrt{g} \mathbf{v}) \right]^{\zeta}$, where ρ_m is the mass density. All lengths are normalized to a generalized minor radius a ; the resistivity to η_0 (its value at the magnetic axis); the time to the poloidal Alfvén time $\tau_{hp} = R_0(\mu_0\rho_m)^{1/2}/B_0$; the magnetic field to B_0 (the averaged value at the magnetic axis); and the pressure to its equilibrium value at the magnetic axis. The Lundquist number S is the ratio of the resistive time $\tau_R = a^2\mu_0/\eta_0$ to the poloidal Alfvén time.

Equilibrium flux coordinates (ρ, θ, ζ) are used. Here, ρ is a generalized radial coordinate proportional to the square root of the toroidal flux function, and normalized to one at the edge. The flux coordinates used in the code are those described by Boozer [5], and \sqrt{g} is the Jacobian of the coordinates transformation. The code uses finite differences

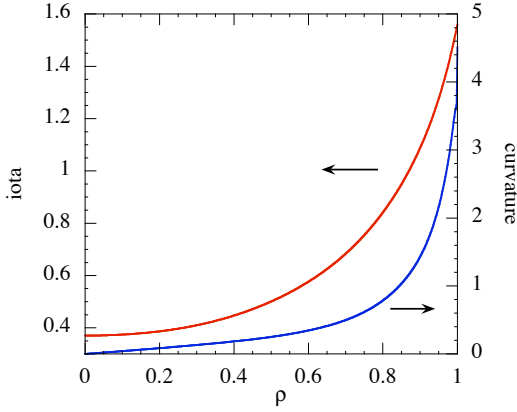


Fig. 1 Equilibrium profiles of the rotational transform and curvature for $\beta_0 = 2 \times 10^{-3}$. The LHD configuration is described in the text.

in the radial direction and Fourier expansions in the two angular variables. The numerical scheme is semi-implicit in the linear terms. The nonlinear version uses a two semi-steps method to ensure $(\Delta t)^2$ accuracy.

3 Linear Results

The method is especially suitable for the study of LHD configurations since they verify the assumptions, and the dominant equilibrium modes are $(m = 1, n = 0)$, and $(m = 2, n = 10)$. We start by studying the linear stability properties of a sequence of zero net-current fixed boundary equilibria with parameters $R_{ax} = 3.6$ m, $B_q = 100\%$, $\gamma = 1.25$, and a pressure profile $p \sim 1 - \rho^2$. The profiles of the rotational transform and curvature for the case with $\beta_0 = 2 \times 10^{-3}$ are shown in Fig. 1. The rotational transform profile changes very slightly for the scan in β . The value of the ideal Mercier stability criterion DI [6] as a function of β_0 at the position of the $\iota = 1/2$ and $\iota = 1$ rational surfaces is shown in Fig. 2. From the Mercier criterion we expect that ideal modes localized at $\iota = 1/2$ are stable for $\beta_0 < 6 \times 10^{-3}$, and those localized at $\iota = 1$ are stable for $\beta_0 < 0.02$. The results of the linear growth rate and the width of the dominant Fourier component ($m = 2, n = 1$) of the $n = 1$ mode are shown in Fig. 3 for the ideal case and the case with $S = 10^7$. In these calculations, we include equilibrium components with $n = 0, 10, 20$, and, consequently, dynamic components with $n = 1, 9, 11, 19, 21$. The mode is ideally stable for $\beta_0 < 8 \times 10^{-3}$, a value close to the one given by the Mercier criterion. The resistive and ideal modes are very localized for β_0 -values below 0.01, and they are very similar for β_0 -values above 0.01.

The effect of the toroidal and helical couplings can be seen in Fig. 4, where the dominant component of the $n = 1$ family is shown for three different linear calculations: When only one dynamical component is included (Cylinder), when only components with $n = 1$ are included

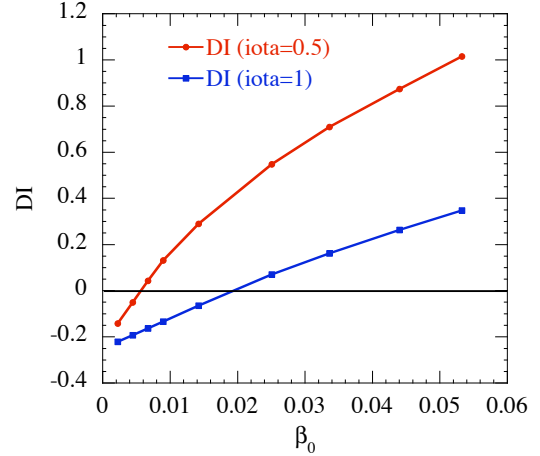


Fig. 2 Values of the ideal Mercier criterion vs. β_0 for the same LHD configuration as in Fig. 1 at the radial position of the $\iota = 1/2$ and $\iota = 1$ rational surfaces.

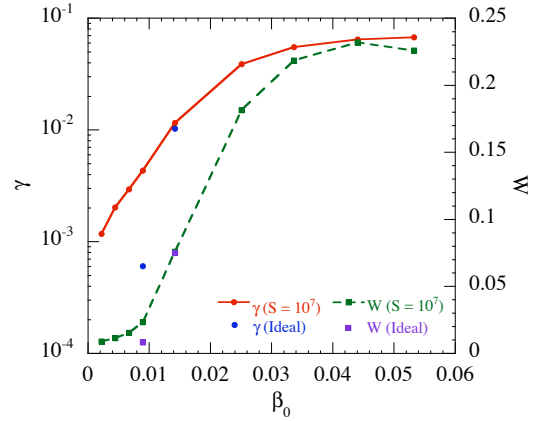


Fig. 3 Ideal and resistive ($S = 10^7$) linear growth rate of the $n = 1$ mode vs. β_0 for the same LHD configuration as in Fig. 1. The width of the dominant ($m = 2, n = 1$) Fourier component is also represented

(Toroidal), and when components with $n = 1, 9, 11$ are included (Helical). The equilibrium parameters of this configuration are $R_{ax} = 3.6$ m, $B_q = 100\%$, $\gamma = 1.25$, $I_p < 0$, and correspond to an experimental discharge with localized oscillations at the $(m = 2, n = 1)$ rational surface [7]. The Lundquist number S is 8×10^7 , and the growth rate increases by more than a factor of 2 from the cylindrical to the full calculation. The dominant radial magnetic field components are shown in Fig. 5. The importance of the helical couplings for the magnetic terms is clear from the Figure.

4 Nonlinear Results

We have followed the nonlinear evolution in the cylindrical and toroidal limit. The value of S in these calculations is reduced in such a way that the linear growth rate and

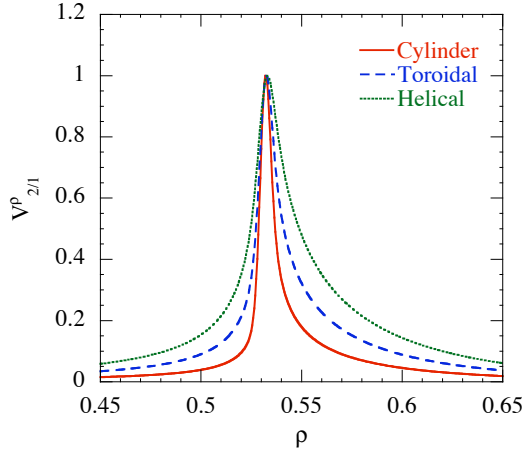


Fig. 4 Comparison of the dominant component of linear eigenfunctions with no couplings, with toroidal couplings, and with toroidal and helical couplings. The LHD configuration is described in the text.

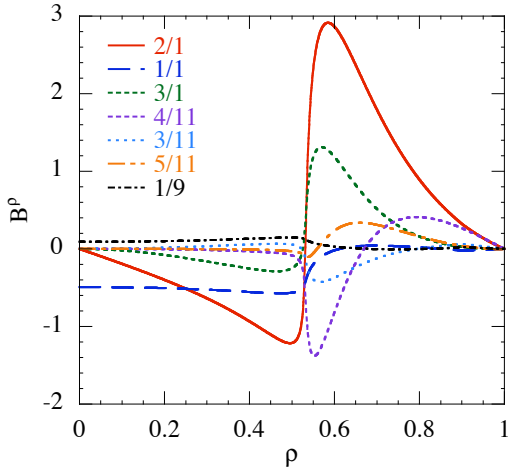


Fig. 5 Dominant radial magnetic field components for the case of Fig. 4 with all the couplings included.

width of the dominant component are similar to those of the linear calculation including helical couplings. The calculation for the cylindrical limit is single-helicity, that is, only components with $m/n = 2$ are included. As can be seen in Fig. 6, the nonlinear evolution for the cylindrical case leads to saturation with bursting activity. The pressure profile flattens around the $\iota = 1/2$ rational surface. For the toroidal limit, the components with the same n are linearly coupled. The saturation level increases with respect to the single-helicity case, and the profile of the root mean squared value of the radial velocity widens with respect to the linear eigenfunction, as can be seen in Fig. 7. In both calculations, the $(m = 2, n = 1)$ component dominates the spectrum. The calculation of the nonlinear evolution including linear helical couplings is under way.

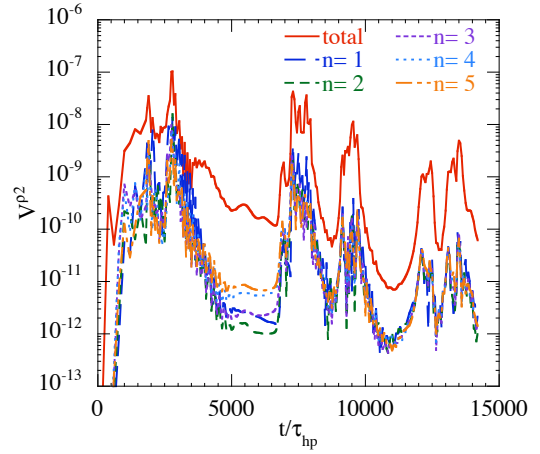


Fig. 6 Nonlinear evolution of the integral of the mean squared value of V^p for the case of Fig. 4.

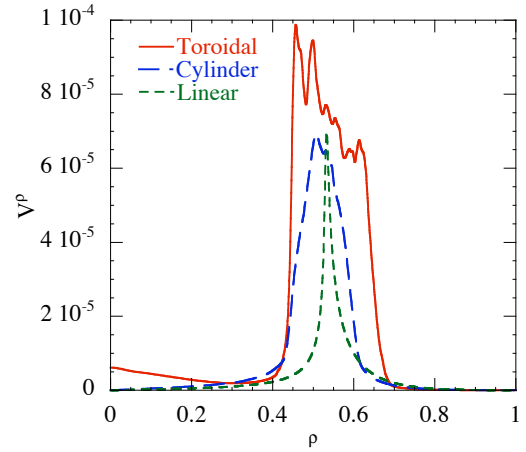


Fig. 7 Comparison of the time-averaged root mean squared value of V^p during the stationary phase for the nonlinear cylindrical and toroidal cases. The linear eigenfunction is also plotted.

5 Pressure-convection Limit

The natural generalization of the set of reduced equations would be to write the velocity and magnetic field as

$$\mathbf{v} = \sqrt{g} [R_0 \nabla \zeta \times \nabla \Phi + \nabla \theta \times \nabla (\rho \Lambda)], \quad (5)$$

$$\mathbf{B} = R_0 \nabla \zeta \times \nabla \psi + \nabla \theta \times \nabla (\rho \chi), \quad (6)$$

where Φ and Λ are velocity stream-functions, and ψ and χ , the perturbations of the poloidal and toroidal flux, respectively. In this formulation, the incompressibility condition is approximate (higher order in the reduced equations), $\nabla \cdot (\mathbf{v} / \sqrt{g}) = 0$. It corresponds to the pressure-convection limit of Ref. [4]. To ascertain the validity of the reduced set of equations for LHD, we have compared the results of linear calculations with those obtained using the full MHD equations in the pressure convection limit. The results practically do not change, and are consistent with the

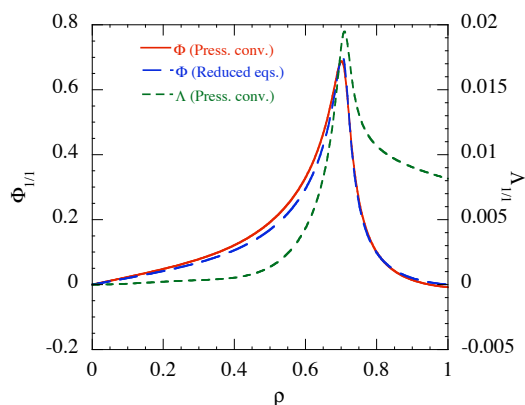


Fig. 8 Comparison of the dominant Fourier component of the stream-function Φ obtained from the reduced and pressure convection limit equations. The stream-function Λ is also plotted using a different scale. The corresponding LHD configuration is described in the text.

approximations made. This is illustrated in Fig. 8 where we have plotted the dominant component ($m = 1, n = 1$) obtained from both calculations for a configuration with aspect ratio 8.3 and $\gamma = 1.13$.

6 Summary

We have derived a set of reduced equations without any assumption on the number of field periods. For the calculation of the linear growth rates and nonlinear evolution, we use Boozer coordinates. The linear results agree very well with the ones obtained from the full MHD equations in the pressure-convection limit. We have studied the nonlinear evolution of the fluctuations in the cylindrical (single-helicity) and toroidal (only $n = 0$ equilibrium modes) limits. The saturated level widens with respect to the linear eigenfunction. The calculation of the nonlinear evolution including linear helical couplings is under way.

One of the authors (L.G.) thanks the staff at NIFS for their support during his stay when part of this work was done.

- [1] L. Garcia, et al., *Phys. Fluids B* **2**, 2162 (1990).
- [2] D.V. Anderson, et al., *Proceedings of Joint Varenna-Lausanne International Workshop on Theory of Fusion Plasmas* (Compositori, Bologna, 1988) p. 93.
- [3] C. Schwab, *Phys. Fluids B* **5**, 3195 (1993).
- [4] L. Garcia, *Proceedings of the 25th EPS International Conference, Prague, 1998*, VOL. 22A, Part II, p. 1757.
- [5] A.H. Boozer, *Phys. Fluids* **25**, 520 (1982).
- [6] C. Mercier, *Nucl. Fusion* **1**, 47 (1960).
- [7] A. Isayama, et al., *Plasma Phys. Control. Fusion* **48**, L45 (2006).